



Lawrence Berkeley Laboratory

UNIVERSITY OF CALIFORNIA

LAWRENCE
BERKELEY LABORATORY

Materials & Molecular Research Division

FEB 24 1982

LIBRARY AND
DOCUMENTS SECTION

Submitted to The Journal of Chemical Physics

VIBRATIONAL RELAXATION OF CH_3F IN INERT GAS MATRICES

Linda Young and C. Bradley Moore

December 1981

TWO-WEEK LOAN COPY

This is a Library Circulating Copy
which may be borrowed for two weeks.
For a personal retention copy, call
Tech. Info. Division, Ext. 6782



LBL-13871
c.2

DISCLAIMER

This document was prepared as an account of work sponsored by the United States Government. While this document is believed to contain correct information, neither the United States Government nor any agency thereof, nor the Regents of the University of California, nor any of their employees, makes any warranty, express or implied, or assumes any legal responsibility for the accuracy, completeness, or usefulness of any information, apparatus, product, or process disclosed, or represents that its use would not infringe privately owned rights. Reference herein to any specific commercial product, process, or service by its trade name, trademark, manufacturer, or otherwise, does not necessarily constitute or imply its endorsement, recommendation, or favoring by the United States Government or any agency thereof, or the Regents of the University of California. The views and opinions of authors expressed herein do not necessarily state or reflect those of the United States Government or any agency thereof or the Regents of the University of California.

VIBRATIONAL RELAXATION OF CH₃F IN INERT GAS MATRICES
~~~~~

Linda Young\* and C. Bradley Moore

Department of Chemistry, University of California  
and Materials and Molecular Research Division of  
the Lawrence Berkeley Laboratory, Berkeley, CA 94720

ABSTRACT  
~~~~~

The deactivation mechanism of the CH stretching fundamentals and bending overtones in matrix isolated CH₃F has been determined for dilute samples as a function of host and temperature using infrared laser excited vibrational fluorescence. The decay mechanism is the same for all hosts; depopulation of any of the levels near 3000 cm⁻¹ occurs via rapid (<5 ns) V → V transfer to the CF stretching overtone level 2ν₃. Subsequent stepwise relaxation occurs from 2ν₃ to ν₃ and from ν₃ to ground. Decay rates of 2ν₃ and ν₃ have been determined through temporal resolution of 1050 and 2100 cm⁻¹ fluorescence, respectively. These rates show a dramatic dependence on host lattice, an increase of two orders of magnitude in going from Xe to Ar matrices. Lifetimes depend only weakly on temperature.

I. INTRODUCTION

~~~~~

Recent studies are leading to a qualitative understanding of the factors governing the mechanism of vibrational relaxation of diatomics isolated in monatomic hosts. Isolated diatomic molecules may dissipate vibrational energy either directly to the host lattice, by simultaneous emission of many bulk phonons, or indirectly, via a local mode with subsequent relaxation to lattice modes. The dominant channel of non-radiative relaxation appears to be the one of lowest order, i.e. that requiring the smallest quantum number change. Hence, low moment of inertia hydrides, e.g.  $\text{HCl}^1$ ,  $\text{NH}_2$ , appear to relax via localized rotational modes, whereas heavy diatomics  $\text{O}_2^3$ ,  $\text{C}_2^{-4}$ , probably relax via local phonon modes.

Relatively little is known about the mechanisms of vibrational relaxation of matrix isolated polyatomics, where the additional channels of intramolecular V-V transfer are present. Most studies to date have been conducted on electronically excited species by observation of vibrationally unrelaxed emission. Inefficient mode-to-mode vibrational energy transfer is observed in the  $\text{ClCF}$  radical/Ar system<sup>5</sup>, in which the bend and high frequency stretch decay independently by multiphonon processes. On the other hand, extremely efficient intramolecular V-V processes dominate the vibrational relaxation within the electronic-

ally excited states of matrix isolated CNN<sup>6</sup> and NCO<sup>7</sup>, such that deactivation of the high frequency stretch proceeds via energy transfer to the bending mode. The drastically different behavior can be explained by allowing efficient energy transfer between levels known to be in Fermi resonance, as are the bending overtones and stretching fundamentals of CNN and NCO.

Even less is known about intramolecular V-V energy transfer in the ground electronic state. The only reported study is that of Abouaf-Marguin et al.<sup>8</sup> where efficient intramolecular V-V transfer ( $<1.6 \mu\text{s}$ ) from the  $\nu_3$  (CF stretch) to the  $\nu_6$  (deformation) was observed in  $^{12}\text{CD}_3\text{F}$  and  $^{13}\text{CD}_3\text{F}$ . This is attributed to the weak Coriolis coupling between the two states and the modest exothermicity of the process. The corresponding process in  $\text{CH}_3\text{F}$  is endothermic and therefore not observed.

Existing data are still too sparse to generalize. Outstanding questions in polyatomic relaxation are 1) the relative importance of inter vs. intramolecular forces during various stages in the relaxation process, 2) the role of symmetry in intramolecular vibrational relaxation, 3) the comparison to relaxation rates in other media, i.e. liquid and gas phase.

$\text{CH}_3\text{F}$  is a particularly useful molecule to study with regard to these questions. The first question is addressed by systematic study of V-V and V-R,P rates as a function of

host lattice. Initial population of symmetric( $A_1$ ) and anti-symmetric( $E$ ) CH stretches and deformation overtones ( $2\nu_2, 2\nu_5$ ) which can be accomplished with a tunable infrared source in the  $3.5 \mu$  region probes the second question. Many lower lying levels are infrared active, thus a mapping of the deactivation path is possible by the observation of vibrational fluorescence. Finally, the deactivation of the lowest lying fundamental,  $\nu_3$ , has been studied in liquid solution<sup>9</sup> as well as in the matrix. Extensive gas phase results are available for both  $V \rightarrow T$ ,  $R$  and  $V \rightarrow V$  processes in  $CH_3F$ .<sup>10</sup>

## II. EXPERIMENTAL

### A. Matrix preparation

Matrices were prepared by deposition of high pressure pulses (50-150 torr, 12 cm<sup>3</sup>, 4 per min) of a premixed gaseous sample onto a CsI target mounted in an Air Products Inc. Model CSA 202 closed cycle helium refrigerator. The spray-on orifice consisted of 1/4 in. OD stainless steel tubing terminated 3/4 in. from the target. The deposition temperatures for Ar, Kr, and Xe hosts were 9, 20 and 25 K, respectively. The temperature of the target could be raised from a minimum temperature of ca. 9 K to 300 K by increasing the effective heat load through resistive heating of a nichrome wire wrapped around the copper block in which the target holder was screwed. The temperature was monitored by a KP vs. Au 0.07 at% Fe thermocouple sandwiched between the CsI target and its holder. Temperature stability ranged from  $\pm 0.3$  K at the lowest temperature to  $\pm 0.1$  K at 40 K.

The gases used were CH<sub>3</sub>F (Matheson, >99.0%), Ar (Matheson Ultra-high Purity >99.995%), Kr (Airco, >99.995%), and Xe (Airco, >99.995%). Kr and Xe were subjected to two freeze-pump-thaw cycles before use. CH<sub>3</sub>F was purified by fractional distillation from 138 K to 77 K. Pressures were measured using a mercury triple McLeod gauge and mercury manometer to better than 2%. Matrix concentrations were assumed to be identical to those of the gaseous mixture.

Absorption spectra of each matrix were taken with a Nicolet 7199 FTIR in order to determine quantitatively the optical densities for absorbing and emitting transitions.

## B. Fluorescence Experiments

~~~~~

The excitation source used in these experiments was a Nd:YAG pumped optical parametric oscillator. The typical pump pulse, produced by a Raytheon SS404 Nd:YAG oscillator amplifier system was 120-150 mJ at 9398 cm^{-1} , 15 ns (FWHM), 0.1 cm^{-1} bandwidth, 1 mrad divergence. Typical output characteristics of the LiNbO_3 parametric oscillator near 3000 cm^{-1} were 1.5 mJ idler energy, 2.0 cm^{-1} FWHM idler linewidth (w/o etalon), 0.2 cm^{-1} FWHM (w/etalon), 8 ns (FWHM), 10 mrad divergence.

A photoconductive Cu:Ge detector was used to monitor infrared fluorescence in these experiments. Changing the external load resistor during the course of the experiment allowed the two complementary configurations: fast response, low sensitivity and slow response, high sensitivity, to be attained without time consuming realignment. The high frequency time constant of each configuration was measured as the response to 2900 cm^{-1} OPO radiation (FWHM = 8 ns). The values obtained were 15 ns and 150 ns for the fast and slow configurations, respectively. The low frequency cut off, measured by chopping a heat lamp and observing the deviation from a square wave, was 2 ms. Cooled interference filters (77 K) were located inside the detector dewar in order to

eliminate the maximum amount of 300 K background radiation. Broadband fluorescence near 1050 cm^{-1} was isolated with a set of two filters having a combined average transmission of 70%, center frequency at 980 cm^{-1} , 10% points at 1132 cm^{-1} and 850 cm^{-1} . Overtone fluorescence near 2100 cm^{-1} was isolated using a set of three filters with a combined average transmission of 59%, center frequency at 2120 cm^{-1} , 10% points of 2030 cm^{-1} and 2220 cm^{-1} (48% transmitting at 2064 cm^{-1} $\text{CH}_3\text{F}/\text{Ar}$ ($2\nu_3 \rightarrow 0$)). Observation of 1500 cm^{-1} fluorescence through a combination of filters and LiF flats yielded $\sim 20\%$ transmission at the ($2\nu_{2,5} \rightarrow \nu_{2,5}$) and ($\nu_{2,5} \rightarrow 0$) transition frequencies.

A schematic of the experimental set up is shown in Fig. 1. The infrared beam was collimated with a single 2 m quartz lens to a spot size of $\sim 1\text{ cm}$ at the sample. A 5 cm f/1 NaCl lens focussed the fluorescence onto the $3 \times 10\text{ mm}$ detector element. Both front (Fig. 1) and rear surface excitation geometries were used in experiments. During rear surface excitation, the infrared beam is directed straight through the sample at the detector. The fluorescence signal was averaged at 10 Hz on a Tektronix 7912AD transient digitizer interfaced to a LSI-11/03 micro-computer. The resultant signals were analyzed by computer as either single or double exponential decays. Uncertainties in single exponential fits were $\pm 5\%$ leading to an overall scatter in data of $\pm 10\%$. Distortion of the signal due to the finite bandwidth of the amplifiers is at most 5%.

III. RESULTS AND ANALYSIS

A. Spectroscopy

The spectroscopy of CH_3F in Ar matrices¹¹ and of the ν_3 region of CH_3F in Kr¹² has been previously reported. Dimeric bands were identified by diffusion and concentration experiments, in agreement with previous studies.¹⁰ The centers of all observable monomeric bands as a function of host are shown in Table I.^{13, 14} A representative spectrum is shown in Fig. 2. The linewidths of the various bands are dependent on the symmetry of the normal mode, as can be seen in the figure and Table II,^{15 - 17} where integrated absorbances and linewidths are listed for each of the bands. The problems in assigning absolute absorption intensities to matrix isolated species are twofold. First, the magnitude of the transition dipole moment of aggregates relative to monomer is generally unknown, thus absolute concentration measurements are not accurate for matrices in which polymer formation is substantial. Next, more dilute matrices suffer from problems in measuring thickness using the interference method, as surfaces parallel to an infrared wavelength are difficult to obtain for thick samples. Moreover, the density of the matrix is dependent upon the deposition temperature,¹⁸ leading to a possible systematic error in concentration measurements. The absolute intensity values shown in Table II are subject to these errors. Since the monomer and dimer contributions to overall band intensity overlap

in some cases and not in others, matrices of high M/A are required to obtain accurate relative intensities. The relative intensities for a dilute matrix, M/A=4940, normalized to the $B_{\text{Obs}}(\nu_3)$ of Barrow and McKean, are therefore also shown. The relative intensities of the "monomer" absorption bands are subject only to errors in baseline determination and the presence of <2% dimer. The data appear nominally consistent with that of the gas phase, but a more reliable set of gas phase cross sections is needed in order to determine whether or not transition dipole moments change between gas and matrix.

The contours of the parallel and perpendicular bands are roughly those expected for a cooled gas phase molecule. The parallel bands ($\Delta J=0$, $\Delta K=\pm 1$) exhibit a strong Q-branch with weak shoulders to the red and blue. A rotational envelope for a perpendicular transition of CH_3F ($\Delta K=\pm 1, \Delta J=0, \pm 1$) in the gas phase at 9 K is $\sim 5 \text{ cm}^{-1}$ FWHM, very similar to the observed 5.2 cm^{-1} of the $\nu_4(\text{E})$ vibration in Ar. Therefore it is suggested that the broad linewidth of the bands of E symmetry is due to unresolved rotational structure. The m-sub level degeneracy is lifted by the crystalline field of the lattice and the vibrational degeneracy by Coriolis coupling. These two factors, combined with line broadening by host-guest interaction serve to obscure the rotational line structure predicted for a cooled gas phase molecule. Similar observations have been made in and interpretation applied to the ammonia-chlorine complex.¹⁹

B. Intramolecular V-V transfer
~~~~~

In Fig. 3, the energy level diagram of CH<sub>3</sub>F is shown. The four accessible bands in the 3000 cm<sup>-1</sup> region:  $\nu_4$ ,  $\nu_1$ ,  $2\nu_2$ ,  $2\nu_5$  are of varying symmetry, (Table I). However, excitation of any of these levels leads to identical relaxation behavior. Each of the four levels was excited in each matrix. Fluorescence is observed only from the  $\nu_3$  (C-F stretch) manifold, both as fundamental and first overtone emission. Using the 150 ns configuration, no emission was observed from the  $\nu_2$ ,  $\nu_5$  or  $\nu_6$  manifolds after averaging 640 shots. The same number of shots produced S/N of 30 for  $2\nu_3$  emission for which the Einstein A coefficient is 0.25 times that of the  $\nu_{2,5} \rightarrow 0$  transition and 3.4 times that of  $\nu_6$ . This null result implies that either relaxation does not occur through these modes or that the product of relaxation time and fraction of energy relaxing through  $\nu_{2,5}$  is less than 2.5 ns, and through  $\nu_6$  less than 17 ns.

The rate of energy transfer to the  $\nu_3$  manifold is monitored by the risetime of the 1050 cm<sup>-1</sup> fluorescence. This is in all cases, Ar, Kr, and Xe hosts at 9 K, similar to the time constant of the detection apparatus, 15 ns, as is shown in Fig. 4. Thus for all matrices  $\tau_{V-V} < 5$  ns.

C. Deactivation of the  $\nu_3$  manifold  
~~~~~

The decay of emission from the ν_3 manifold was

monitored with the slow, high sensitivity detector configuration. Overtone fluorescence ($2\nu_3 \rightarrow 0$, 2100 cm^{-1}) in all samples decayed as a single exponential, as shown in Fig. 5a. However, fundamental (1050 cm^{-1}) fluorescence decayed as a double exponential, as seen in Fig. 5b. In the analysis, it is assumed that the two components of the decay are due to the transitions $2\nu_3 \rightarrow \nu_3$ and $\nu_3 \rightarrow 0$. Thus, the rate of the fast component of the signal is fixed by the $2\nu_3$ lifetime measured from the overtone fluorescence signal.

Excitation on the front surface of the matrix yielded rates identical to those obtained for excitation on the rear surface. The ratio of the amplitude of the fast to that of the slow component of the broadband decay, A_f/A_s , decreased upon switching from back to front surface excitation. This would be expected since optical attenuation of $\nu_3 \rightarrow 0$ emission during passage through the matrix would occur to a greater extent in the rear surface excitation geometry, where the matrix itself serves as a filter absorbing $1 \rightarrow 0$ emission.

D. Host dependence of the deactivation rates
~~~~~

In Fig. 6 the dependence of the  $\nu_3$  and  $2\nu_3$  lifetimes on host lattice is shown. The rates, plotted as a function of the gas-matrix vibrational frequency shift,

increase almost two orders of magnitude when going from Xe to Ar. This shows that the forces causing relaxation are correlated to those near the equilibrium position of the  $\text{CH}_3\text{F}$  in the host lattice.

E. Temperature dependence of relaxation rates  
~~~~~

In Fig. 7 the temperature dependence of the $2\nu_3$ deactivation rate is shown for the various matrices. The absence of a dramatic dependence on temperature suggests that the relaxation does not proceed via a multiphonon mechanism.²⁰ In Fig. 8 the temperature dependence of the ν_3 relaxation rate is shown. The trends observed for $2\nu_3$ are also observed for ν_3 .

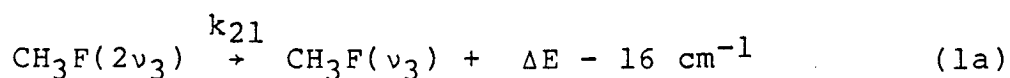
F. Concentration dependence of relaxation rates
~~~~~

In Fig. 9 the concentration dependence of the lifetimes of  $2\nu_3$  and  $\nu_3$  is shown for  $\text{CH}_3\text{F}$  in Ar. The  $\nu_3$  lifetime is seen to increase by a factor of 2 when M/A increases from 1000 to 9750, whereas the  $2\nu_3$  lifetime remains constant within experimental error.

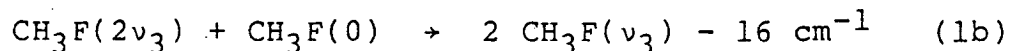
#### IV. DISCUSSION

The important features of CH<sub>3</sub>F isolated molecule vibrational relaxation are as follows: 1) Relaxation from any of the levels,  $\nu_4$ ,  $\nu_1$ ,  $2\nu_2$  or  $2\nu_5$ , proceeds through rapid energy transfer to the  $\nu_3$  manifold. 2) There is a small increase of the  $\nu_3$  relaxation rate as a function of temperature. 3) There is a dramatic effect of host lattice on the relaxation rates of  $\nu_3$  and  $2\nu_3$ . 4) CD<sub>3</sub>F relaxes an order of magnitude more slowly than CH<sub>3</sub>F.

The observed fluorescence decays show that  $2\nu_3$  decays by



and/or



The relaxation is completed by



where  $\Delta E = \nu_3/c = 1040 \text{ cm}^{-1}$  in Ar.

##### A. Mechanism of isolated molecule relaxation

After initial population of one of the  $3000 \text{ cm}^{-1}$  levels, energy may be transferred to any of a number of lower lying levels, as seen in Fig. 3. Endothermic processes are ex-

tremely improbable relative to exothermic ones; rates of one phonon endothermic processes being proportional to  $\bar{n}(\omega) = [\exp(-\hbar\omega/kT)/(1-\exp(-\hbar\omega/kT))]$  compared to  $1+\bar{n}(\omega)$  for exothermic one phonon processes. A transition to  $3\nu_3$  is in all cases endothermic; the endothermicity ranges from  $\sim 50 \text{ cm}^{-1}$  for  $\nu_4$  excitation to  $\sim 200 \text{ cm}^{-1}$  for  $2\nu_2$  excitation. Thus the observed transfer into the  $\nu_3$  manifold must occur via the  $2\nu_3$  level. The fluorescence signal at  $2100 \text{ cm}^{-1}$  is due solely to the decay of the  $2\nu_3$  level and is described by

$$S_2 = gA_{20}N_0 \exp(-k_{21}t). \quad (3)$$

The broadband fluorescence observed at  $1050 \text{ cm}^{-1}$  is the sum of  $(2\nu_3 \rightarrow \nu_3)$  and  $(\nu_3 \rightarrow 0)$  emission. The broadband signal is then

$$S_{bb} = gN_0 \left\{ [A_{21} - \delta\xi A_{10}k_{21}/(k_{21}-k_{10})]\exp(-k_{21}t) + [\delta\xi A_{10}k_{21}/(k_{21}-k_{10})]\exp(-k_{10}t) \right\} \quad (4)$$

where  $g$  = geometrical factor,

$\delta$  = optical density factor (varying from 0 to 1 as the sample goes from opaque to transparent)

$\xi$  = V-V equilibration parameter (varying from 1 to 2 as the percentage of molecules decaying by Process (1a) goes from 100% to 0%)

$A_{20}, A_{10}, A_{21}$  = Einstein A coefficients for  $2 \rightarrow 0$ ,  $1 \rightarrow 0$  and  $2 \rightarrow 1$  transitions, respectively.

Assuming  $A_{21} = 2A_{10}$  we can derive an expression for the product  $\delta\xi$  which can be evaluated from measured rate and amplitude ratios

$$\delta\xi = [2/(A_f/A_s - 1)]x(1 - k_{10}/k_{21}). \quad (5)$$

For the rear surface excitation geometry  $\delta$  can be evaluated for the particular mode excited using a simple one dimensional model in which non-uniform excitation and emission according to Beer's Law is taken into account

$$\delta = \frac{\int_0^l N_0 \exp(-\gamma_{ex}(1-x)) x \exp(-\gamma_{em}x) dx}{\int_0^l N_0 \exp(-\gamma_{ex}x) dx} \quad (6)$$

where  $\gamma_{ex}$ ,  $\gamma_{em}$  are defined by Beer's Law,  $I/I_0 = \exp(-\gamma l)$ . Observed values for a broadband signal resulting from rear surface excitation of the  $\nu_4$  mode of  $\text{CH}_3\text{F}$  in Ar are  $k_{10} = 3.2 \times 10^5 \text{ s}^{-1}$ ,  $k_{21} = 1.30 \times 10^6 \text{ s}^{-1}$  and  $A_f/A_s = 6.5 \pm 1.5$ . These numbers yield a value for  $\delta\xi = 0.27 \pm 0.1$ . From the absorption spectrum, the value of  $\delta$  is determined from the emitting  $\nu_3$  band of this particular matrix to be 0.26. This implies that  $\xi = 1.0 \pm 0.4$  and that (1a) is dominant, i.e. that endothermic intermolecular V-V processes are not very probable. The lack of a dramatic concentration dependence of  $\tau(2\nu_3)$  further supports a relaxation mechanism in which intermolecular V-V processes are unimpor-

tant in the deactivation of  $2\nu_3$ . In addition, if (1b) were dominant one would expect a similar temperature dependence for  $k_{21}$  in all hosts since the endothermicity of the V-V process is essentially equal for Ar, Kr and Xe ( $\Delta E \sim 16 \text{ cm}^{-1}$ ). However, this is not observed, the variation of rate with temperature being much greater in Xe than in Ar. Furthermore, the predicted temperature dependence of an endothermic  $16 \text{ cm}^{-1}$  process,  $\Gamma \propto n(\omega)$ , is much greater than that observed for any host. The values reported in Table III are isolated molecule relaxation rates for  $\nu_3$  and  $2\nu_3$ .

The  $\nu_3$  lifetimes are in good agreement with those of Abouaf-Marguin and Gauthier-Roy<sup>8</sup> and with the less direct measurements of Apkarian and Weitz.<sup>21</sup> In the latter study strong pumping of  $\nu_3 \nu=0 \rightarrow 1$  led to population of higher levels within the  $\nu_3$  manifold via exothermic intermolecular V-V processes. Overtone emission near  $5 \mu$  was observed from molecules situated such that V-V transfer is faster than  $k_{10}$ . In such a V  $\rightarrow$  V coupled system  $\text{CH}_3\text{F}(2\nu_3)$  should, and did, relax at a rate equal to  $2k_{10}$  since its concentration is proportional to the square of the  $\text{CH}_3\text{F}(\nu_3)$  concentration.<sup>21</sup> Since  $2\nu_3$  is populated before  $\nu_3$  in the present study, the reported relaxation rates probe a different population distribution within the  $\nu_3$  manifold and a different set of molecules, i.e. ones for which  $\text{CH}_3\text{F}(2\nu_3)$  is isolated with respect to resonant V  $\rightarrow$  V transfer to  $\text{CH}_3\text{F}(\nu_3)$ .<sup>22</sup>

B. Temperature dependence  
~~~~~

A mechanism in which rotation is the dominant accepting mode, with the excess energy being absorbed by bulk modes, has been proposed to explain the deactivation of the ν_3 level.⁸ In this model, the vibrational energy is converted to the maximum amount of rotational energy consistent with exothermicity requirements. To minimize the quantum number change for CH_3F , rotation about the symmetry axis is assumed. For CH_3F this corresponds to a final rotational quantum number of $J=14$. Perturbations of this level by the matrix are expected to be small as an analysis of the ν_3 parallel band has shown that the barrier to rotation about the symmetry axis is quite small in all hosts.^{8, 22} The temperature dependence of the relaxation rate can then be primarily attributed to the emission rate of one or two phonons at the mismatch frequency. The calculated temperature dependence of a process which requires the emission of one bulk phonon of frequency ω is¹

$$k \propto [\bar{n}(\omega) + 1]. \quad (7)$$

The calculated dependence of rate on temperature, normalized to 9 K, is shown in Figs. 7 and 8 for various phonon frequencies. The temperature variation of rates can be fit quite well with processes requiring the emission of one bulk phonon. The phonon frequency required to fit the temperature dependence systematically decreases in the series Ar, Kr, Xe as

does the magnitude of the $2\nu_3 \rightarrow \nu_3$ transition frequency. The trend is also present in the ν_3 relaxation rates. It is not possible to correlate the absolute magnitude of the phonon frequency which best fits the observed temperature dependence with the energy mismatch between the final and initial states as the spectroscopy of high J states in matrices is unknown.

C. Host effect

~~~~~

The relaxation rates of both  $\nu_3$  and  $2\nu_3$  show a dramatic dependence on host lattice, the rates in Ar being a factor of 30 greater than those in Xe. The trend of increasing rate with decreasing host size is consistent with a model in which short range repulsive forces are responsible for inducing relaxation, similar to the gas phase description, where a binary collision model is used to explain the relaxation.

For an extrapolation between phases to be meaningful, the relaxation probability per collision should be constant for identical collision partners. The relaxation probability of  $\text{CH}_3\text{F}(\nu_3)$  in liquid Ar at 77 K<sup>9</sup> and in gas phase at 300 K<sup>10</sup> can be compared using a cell model for the collision frequency in the liquid phase,

$$Z = (8kT/\pi m)^{1/2} \times [ 2^{1/6}/\rho^{1/3} - \sigma^{1/2} ]$$

where  $m = \text{CH}_3\text{F}$  mass,  $\rho = \text{liquid number density}$ ,  $\sigma = \text{collision}$

cross section.  $Z$  at 77 K is  $3 \times 10^{12} \text{ s}^{-1}$ . The values obtained for the relaxation probability are  $P_{\text{CH}_3\text{F-Ar}}^{\text{liq}}(77\text{K}) = 2.6 \times 10^{-7}$  and  $P_{\text{CH}_3\text{F-Ar}}^{\text{gas}}(300\text{K}) = 5.1 \times 10^{-6}$ . The larger probability is certainly to be expected for the higher temperature. When  $kT$  is less than the two-body well depth, attractive forces influence the relaxation. For  $\text{CH}_3\text{F}/\text{Ar}$ , the well depth estimated from transport data is  $\sim 200 \text{ K}$ . Thus the gas phase 77 K probability cannot be predicted well enough from theory to allow the effect of phase change to be estimated. A comparison between the liquid and solid data is more meaningful.

In the solid phase, the additional problem of defining a "collision" is present. The collision frequency can be estimated from the zero point motion of the guest. The frequency of this mode is estimated to be  $80 \text{ cm}^{-1}$  by fitting a harmonic oscillator potential to the two-body Lennard Jones potential near the minimum. A collision frequency of  $4.8 \times 10^{12} \text{ s}^{-1}$  is obtained after multiplying by a factor of four to account for 2 turning points and 2 translational modes effective in relaxation. The relaxation probability is then calculated to be  $6 \times 10^{-8}$  at 9 K and at 20 K for  $\text{CH}_3\text{F-Ar}$ , about four times smaller than the 77 K liquid phase value obtained for the calculated collision frequency of  $3 \times 10^{12} \text{ s}^{-1}$ . The rates in the matrix show no great dependence on temperature, Fig. 8. Indeed, the temperature dependence due to the emission of a  $30 \text{ cm}^{-1}$  phonon results in an in-

crease in relaxation probability of a factor of two between 9 and 77 K when a constant collision frequency is assumed. Thus the change in phase from solid matrix to liquid changes the relaxation probability by less than a factor of four. It may be more sensible to compare rates rather than relaxation probabilities derived from these crude estimates of collision frequencies. The relaxation rates in a matrix ( $3.2 \times 10^5 \text{ s}^{-1}$  at 9 K and  $3.4 \times 10^5 \text{ s}^{-1}$  at 20 K) and in a liquid ( $7.8 \times 10^5 \text{ s}^{-1}$  at 77 K) are more nearly identical than the estimated relaxation probabilities. Therefore, the effect of solid-liquid phase change on vibrational relaxation rates is less than a factor of two. The physical models for vibrational relaxation in liquid and matrix should be nearly identical.

V. SUMMARY AND CONCLUSIONS

~~~~~

In this work, the mechanism of relaxation from the CH stretching fundamentals and bend overtones in matrix isolated CH₃F has been determined as a function of host and temperature. Despite differences in symmetry and intramolecular coupling, all levels near 3000 cm⁻¹ relax in less than 5 ns for all hosts and temperatures studied by rapid intramolecular V → V transfer to the 2ν₃, CF stretch overtone. The rates of subsequent steps of deactivation of the ν₃ manifold, CH₃F(2ν₃) → CH₃F(ν₃) and CH₃F(ν₃) → CH₃F(0), exhibit a dramatic variation with host and a weak dependence on temperature. In all cases, the deactivation rates measured are non-radiative, the radiative lifetime of ν₃, 67 ms, being roughly 500 times longer than the longest lifetime measured.

The trend of decreasing relaxation rates with increasing in host mass may be qualitatively explained by a model in which hard collisions with the repulsive wall of a lattice atom are responsible for the relaxation. This gas-like collision model may also be useful in the liquid phase.

ACKNOWLEDGMENTS

~~~~~

This research was supported by the U.S. Army Research Office, Triangle Park, N.C. and the Director, Office of Energy Research, Office of Basic Energy Sciences, Chemical Sciences Division of the U.S. Department of Energy under Contract Number W-7405-ENG-48. LY appreciates fellowship support from the National Science Foundation.

REFERENCES

~~~~~

*Present address: James Franck Institute, University of Chicago, 5640 Ellis Avenue, Chicago, IL 60637

1. J. M. Wiesenfeld and C. B. Moore, J. Chem. Phys. 70, 930 (1979).
2. V. E. Bondybey and L. E. Brus, J. Chem. Phys. 63, 794 (1975).
3. R. Rosetti and L. E. Brus, J. Chem. Phys. 71, 3963 (1979).
4. L. E. Brus and V. E. Bondybey, J. Chem. Phys. 63, 3123 (1975).
5. V. E. Bondybey and J. H. English, J. Chem. Phys. 66, 4237 (1977).
6. V. E. Bondybey and J. H. English, J. Chem. Phys. 67, 664 (1977).
7. V. E. Bondybey and J. H. English, J. Chem. Phys. 67, 2868 (1977).
8. L. Abouaf-Marguin and B. Gauthier Roy, Chem. Phys. (in press).
9. S.R.J. Brueck, T.F. Deutsch, and R.M. Osgood, Chem. Phys. Lett. 51, 339 (1977).
10. E. Weitz and G. Flynn, Adv. Chem. Phys. 47, 185 (1981).
11. A. J. Barnes et al, J. Chem. Soc. Faraday Trans. II, 738 (1972).
12. L. Abouaf-Marguin et al, Chem. Phys. 23, 443 (1977).

13. G. Herzberg, Infrared and Raman Spectra, Van Nostrand Reinhold Co., New York (1945).
14. W. C. Smith and I. M. Mills, J. Mol. Spec. 11, 11 (1963).
15. S. Saeki et.al., Spectrochimica Acta 32A, 403 (1976).
16. G.D. Barnett, Thesis, University of Washington (1957).
17. G. M. Barrow and D. C. McKean, Proc. Roy. Soc. (London) A213, 27 (1952).
18. W. Schulze and D. M. Kolb, J. Chem. Soc. Faraday Trans. 2 70, 1098 (1974).
19. G. Ribbegård, Chem. Phys. Lett. 25, 333 (1974).
20. J. Jortner, Molecular Physics 32, 399 (1976).
21. V. A. Apkarian and E. Weitz, Chem. Phys. Lett. 76, 68 (1980)
22. Apkarian and Weitz, private communication.

Table I. Absorption band centers of CH₃F in various matrices^{a,b} at 9 K.

Assignment	gas ^c	Ar	Kr	Xe
$\nu_3(A_1)$	1048.2	1040.0	1035.4	1030.1
$\nu_6(E)$	1195.5	1183	1180	1177
$\nu_2(A_1)$	1475.3	1463	1459	1455
$\nu_5(E)$	1471.1			
$2\nu_3(A_1)$	2081 ^d	2064.5	2055.5	2044.0
$2\nu_5, \nu_2 + \nu_5(E)$		2914 ± 1	2909 ± 1	2900 ± 1
$2\nu_5(A_1)$	2861.6	2863.7	2855.9	2846.5
$2\nu_2(A_1)$				
$\nu_1(A_1)$				
$\nu_4(E)$	2982.2	3017.8	3009.0	2996.5

a. (A₁), (E) denote gas phase symmetries

b. Frequencies of transitions of A₁ symmetry are accurate to ± 0.1 cm⁻¹ of E symmetry to ± 0.5 cm⁻¹

c. Ref. 13

d. Ref. 14

Table II. Integrated absorption coefficients of bands of CH₃F in (cm²/mmol)

Band	$\Delta\nu_{1/2}$ (cm ⁻¹)	A _{total} ^a	A _{corr} ^b	A _{norm}	A _{norm} ^{mon} ^c	A _{gas}
ν (A ₁)	0.5	8660 ± 400	9010	11900	11900	11900, ^d 10400, ^e 9550 ^f
ν_6 (E)	~3.0	118 ± 10 ^g	122	161	125 ^g	177, ^d 145, ^e 276 ^f
ν_2 (A ₁)						
ν_5 (E)	~1.9 ^h	870 ± 100	904	1190	1540	1030, ^d 714, ^e 977 ^f
2 ν_3 (A ₁)	0.9	153 ± 14	159	210	164	
2 ν_2 + ν_5 (E)	4.0	164 ± 20 ^g	170	224	174 ^g	
2 ν_5 (E)						
2 ν_2 (A ₁)	0.7	787 ± 40	818	1080	1290	8320, ^d 6320, ^e 8490 ^f
2 ν_5 (A ₁)						
ν_1 (A ₁)						
ν_4 (E)	5.2	2570 ± 460	2670	3520	4220	

a. Measured from CH₃F/Ar = 1/516, λ = 3.56 x 10⁻³ cm, ρ (T_{dep} = 10 K) = 2.4 x 10²² cm³. Absorber concentration assumed same as gas phase mixture. Length calculated from interference fringes in FTIR spectrum, assuming n_{Ar} = 1.3.

Table II. Integrated absorption coefficients of bands of CH₃F in (cm/mmol)
(continued)

- b. Concentration correction made assuming transition dipole moment of monomer and dimer are equal. Refractive index correction is made assuming $n_{Ar} = 1.3$; $B_{Obs}(s)/B_{Obs}(g) = (1/n)[(n^2+2)/3]^2 (\nu_s/\nu_g)$.
- c. Relative intensities observed for CH₃F/Ar = 1/4940, $A_d/A_m < 0.02$, after annealing.
- d. Reference 17.
- e. Reference 16.
- f. Reference 15.
- g. Calculated from relative intensity to 2ν₃ band observed in M/A = 1000 matrix.
- h. Δν could be due primarily to ν₂(A₁) mode, since ν₂ and ν₅ are overlapped and the relative intensities unknown.

Table III. Isolated molecule decay rates of $2\nu_3$ and ν_3 in various hosts at 9 K.

	Ar	Kr	Xe
$k(2\nu_3)\text{ms}^{-1}$			
This work	1200 ± 120	330 ± 30	33 ± 3
$k(\nu_3)\text{ms}^{-1}$			
This work	320 ± 40	88 ± 10	13 ± 2
Ref. 8	330 ± 30	87 ± 8	17 ± 2

FIGURE CAPTIONS
~~~~~

Figure 1. General experimental schematic shown for front surface excitation. An interference filter (at 77 K) is located inside the detector dewar to spectrally resolve the fluorescence.

Figure 2. Absorption spectrum of  $\text{CH}_3\text{F}/\text{Ar} = 1/1000$ , 9.9 mmol, 9 K deposition;  $\text{CH}_3\text{F}/\text{Ar} = 1/9750$  (bottom-right only). D = dimer. P = polymer.

Figure 3. Energy level diagram for matrix isolated  $\text{CH}_3\text{F}$ . Dashed levels are not observed spectroscopically. Solid arrows indicate laser excitation. Wiggly arrows denote levels detected in emission.

Figure 4. Risetime of  $1050 \text{ cm}^{-1}$  fluorescence for excitation of  $\nu_4$   $\text{CH}_3\text{F}/\text{Ar} = 1/9750$ , 9 K;  $\text{CH}_3\text{F}/\text{Kr} = 1/9810$ , 9 K;  $\text{CH}_3\text{F}/\text{Xe} = 1/10800$ , 9 K.

Figure 5. Rear surface excitation at  $2959.8 \text{ cm}^{-1}$ ,  $\text{CH}_3\text{F}/\text{Kr} = 1/9810$ , 9 K. Curves for  $2\nu_{2,5}$ ,  $\nu_1$  excitation are all identical.

(a)  $2\nu_3 \rightarrow 0$  fluorescence

(b) Broadband  $1050 \text{ cm}^{-1}$  fluorescence

Figure 6. Variation of  $2\nu_3$  and  $\nu_3$  relaxation rates with gas to matrix shift. Abscissa is calculated from values given in Table I.

Figure 7. Temperature dependence of  $2\nu_3$  relaxation rates.  $\text{CH}_3\text{F}/\text{Ar} = 1/9800$ ,  $T_{\text{dep}} = 9$  K, 37 mmoles;  $\text{CH}_3\text{F}/\text{Kr} = 1/9800$ ,  $T_{\text{dep}} = 20$  K, 54 mmoles;  $\text{CH}_3\text{F}/\text{Xe} = 1/11,000$ ,  $T_{\text{dep}} = 25$  K, 37 mmoles. Solid lines are calculated temperature dependences for processes involving the emission of one phonon of frequency  $\nu$ . Values of  $\nu$  are shown on graph.

Figure 8. Temperature dependences of  $\nu_3$  relaxation rates for the same samples as in Fig. 8. Solid lines are calculated temperature dependences for processes involving the emission of one phonon of frequency  $\nu$ . Values of  $\nu$  are shown on graph.

Figure 9. Concentration dependence of  $\tau(\nu_3) = \tau_1$  and  $\tau(2\nu_3) = \tau_2$  for  $\text{CH}_3\text{F}$  in Ar at 9 K. Points are the average of between 4 and 23 decay curves with error bars given as 95% confidence limits.

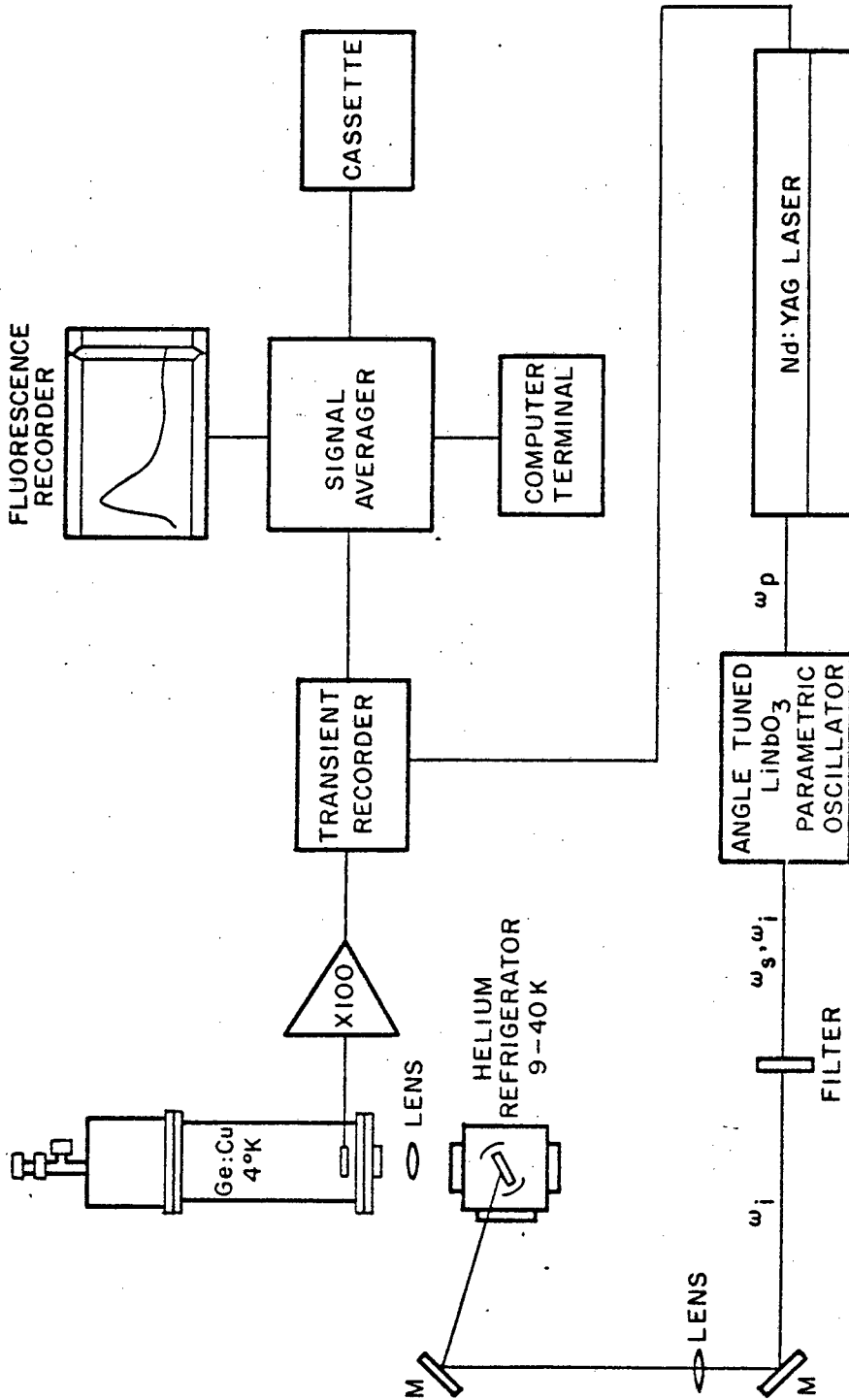


Fig. 1



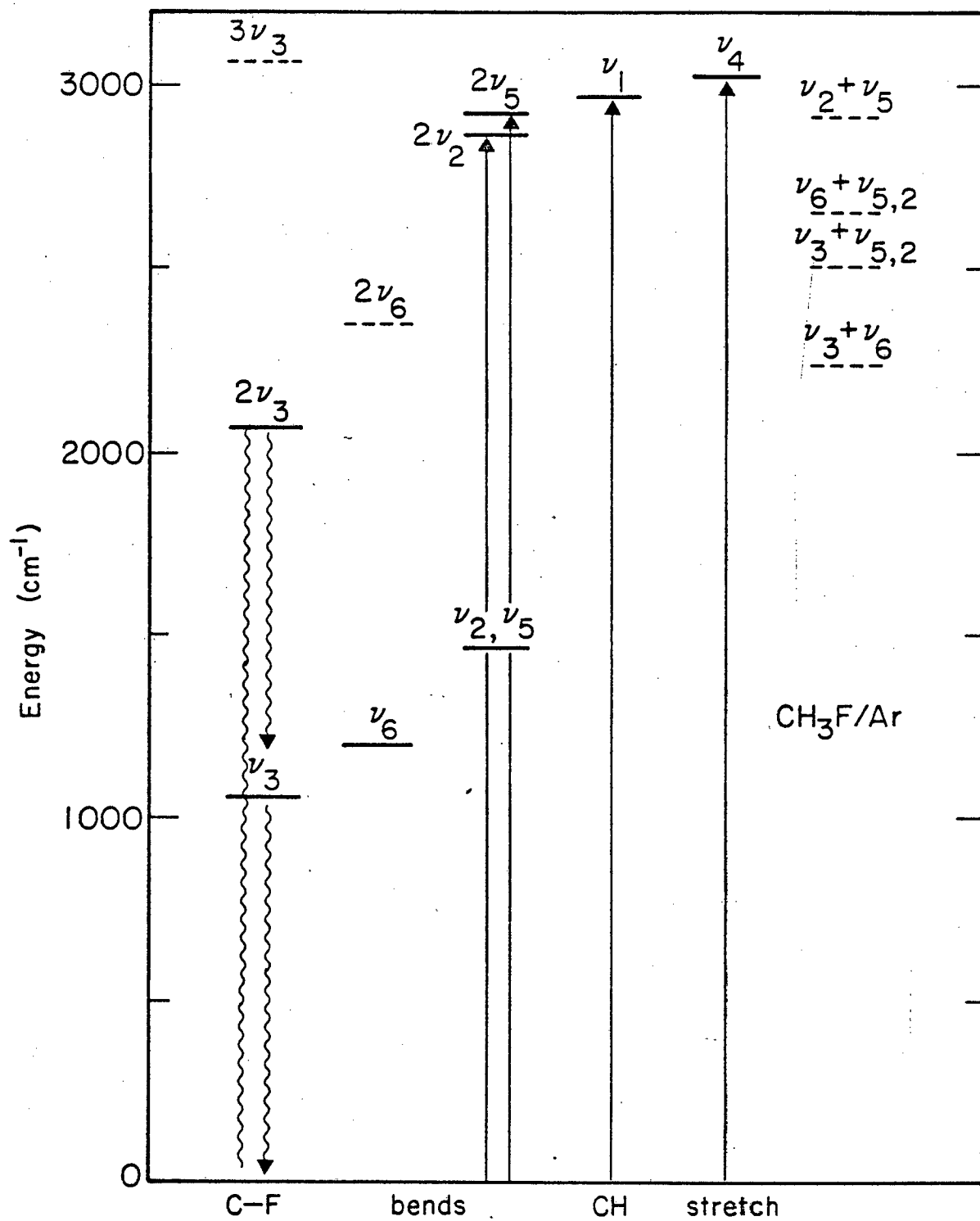


Fig. 3

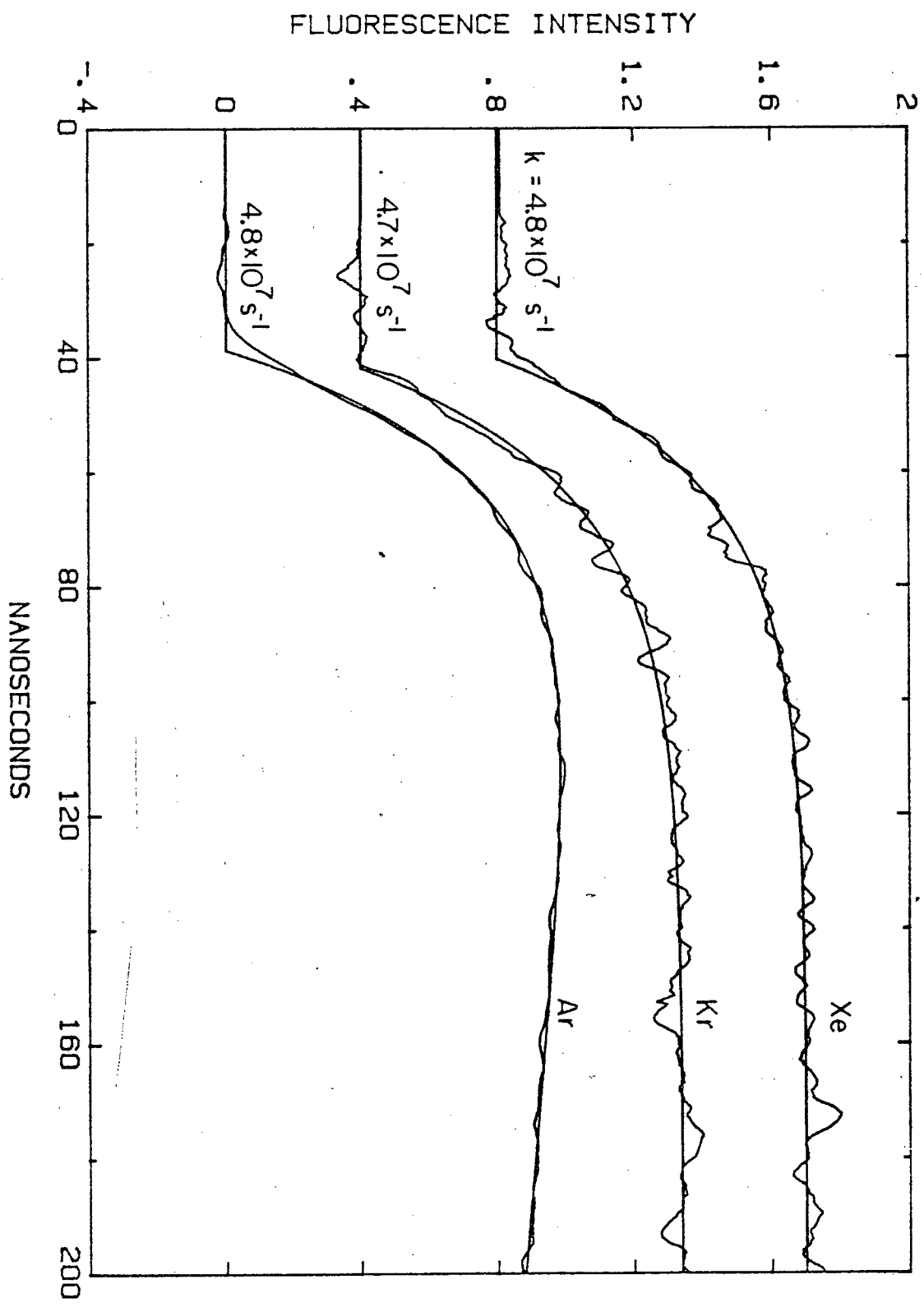


Fig. 4

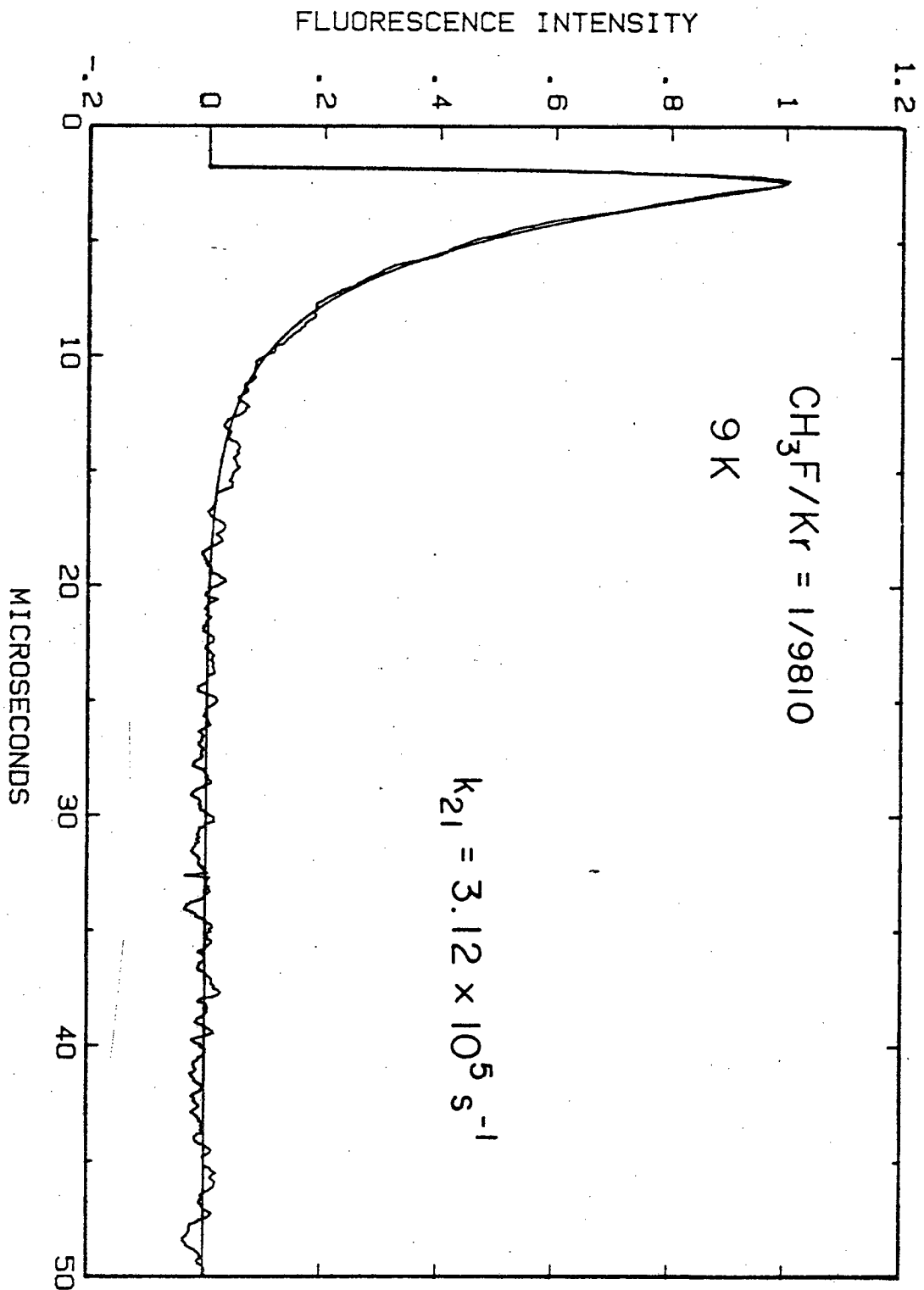


Fig. 5(a)

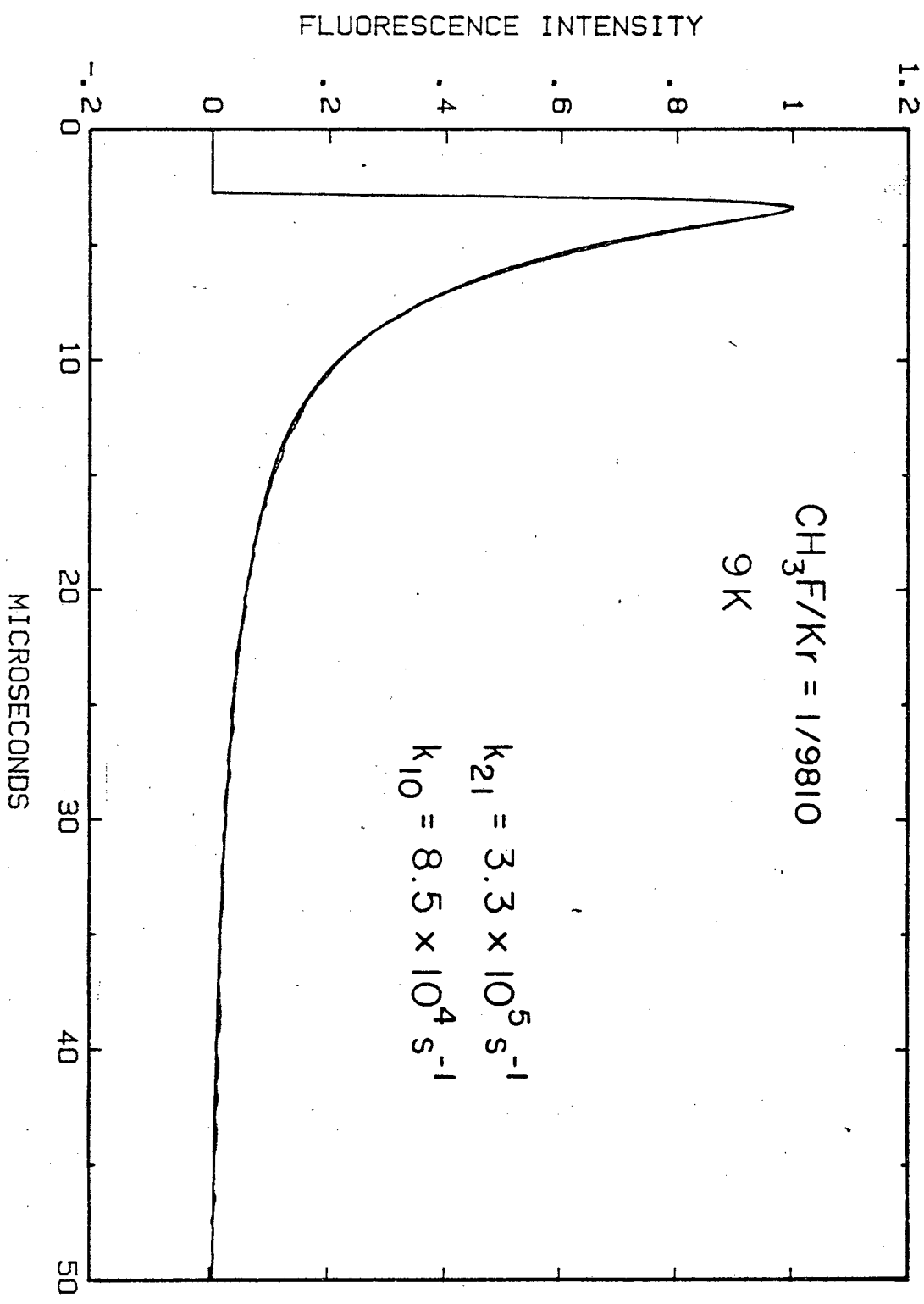


Fig.5(b)

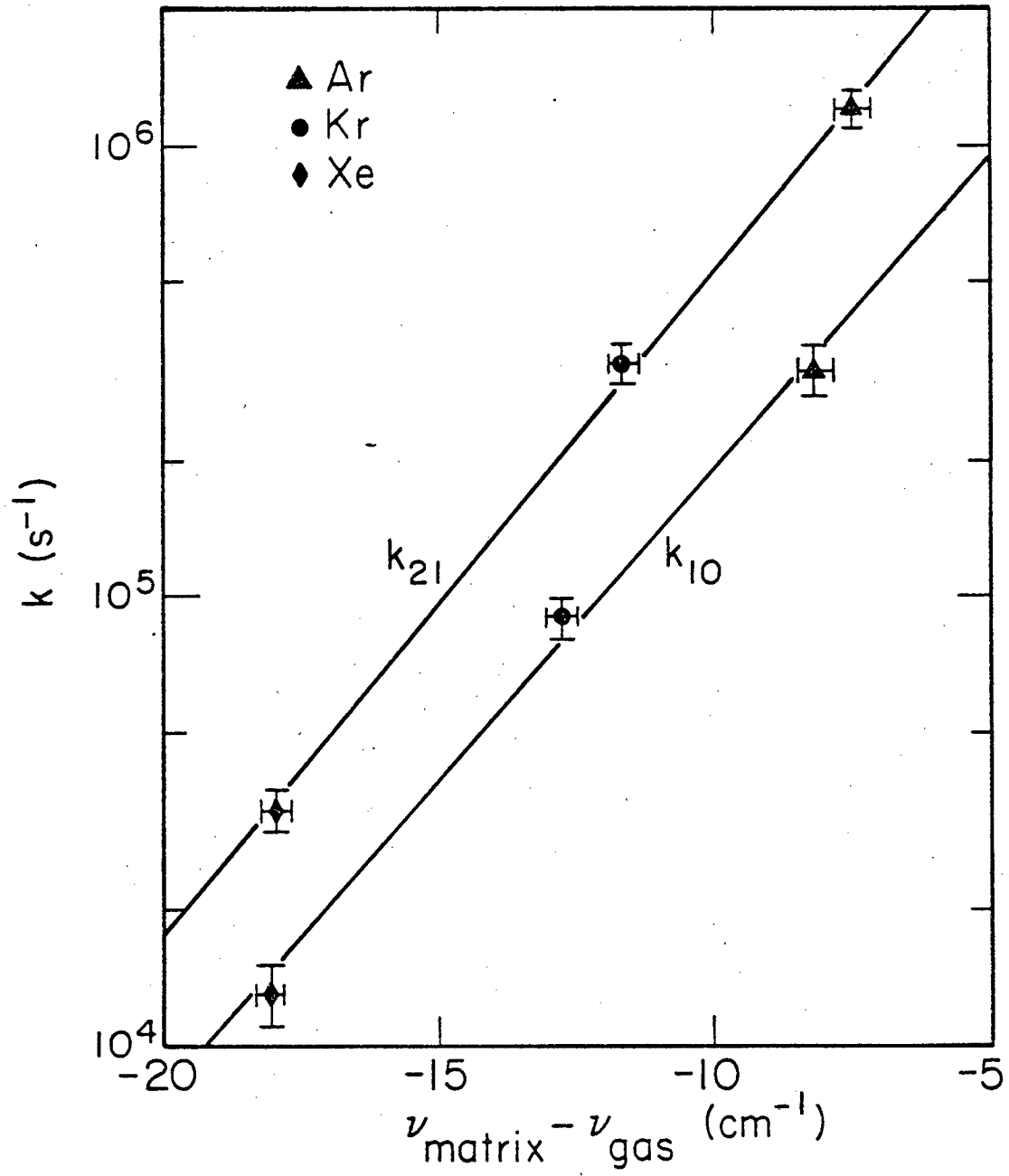


Fig. 6

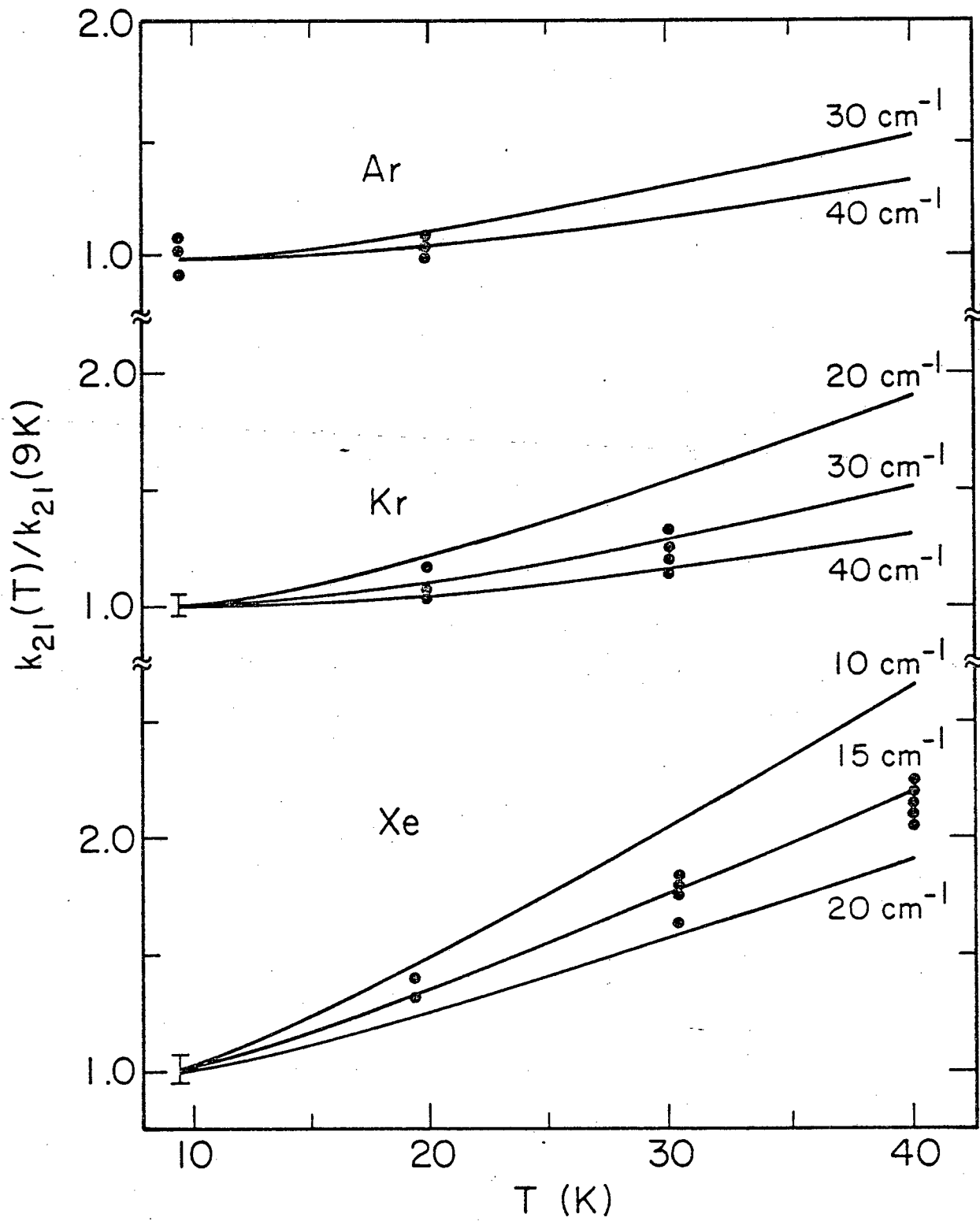


Fig. 7

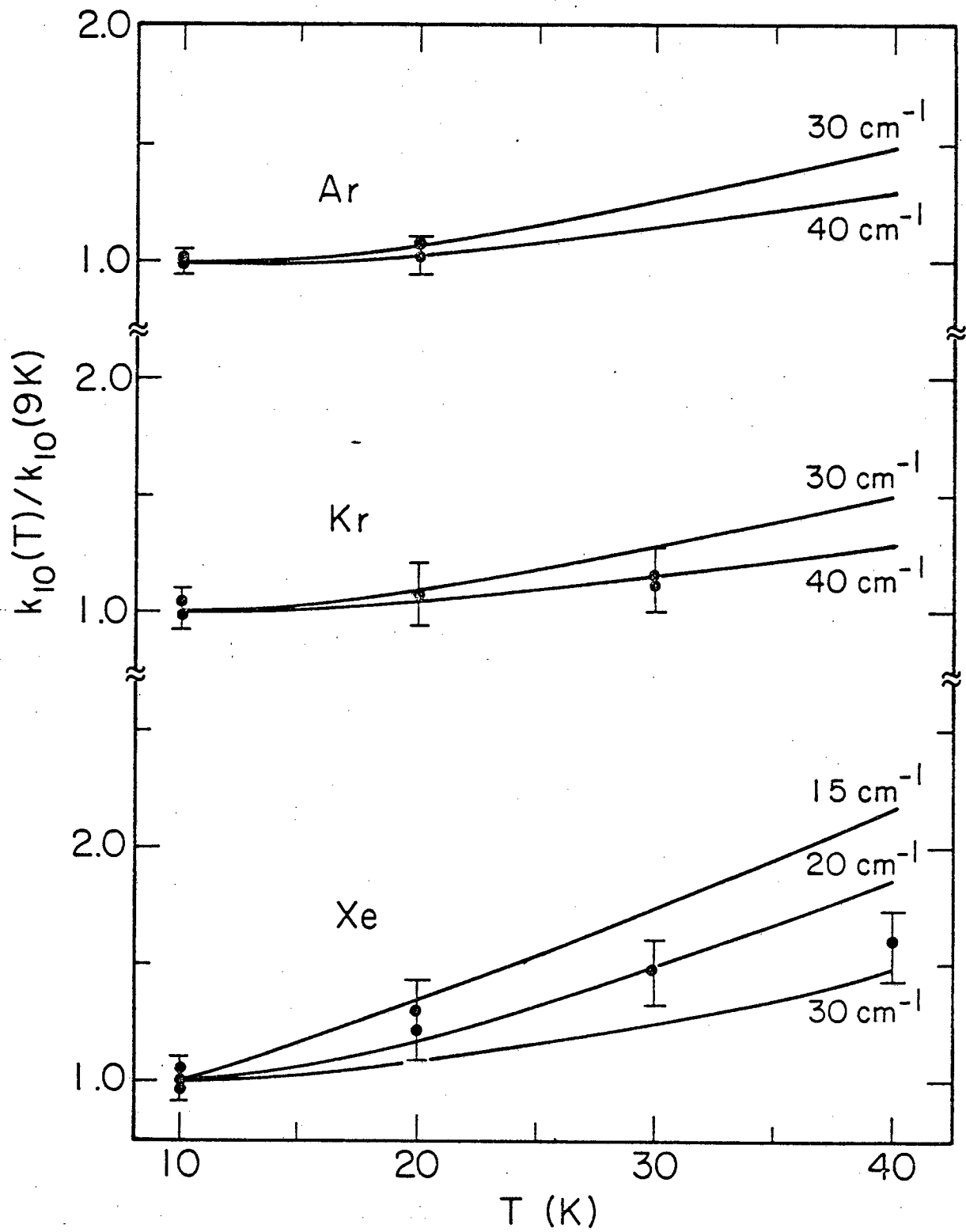


Fig. 8

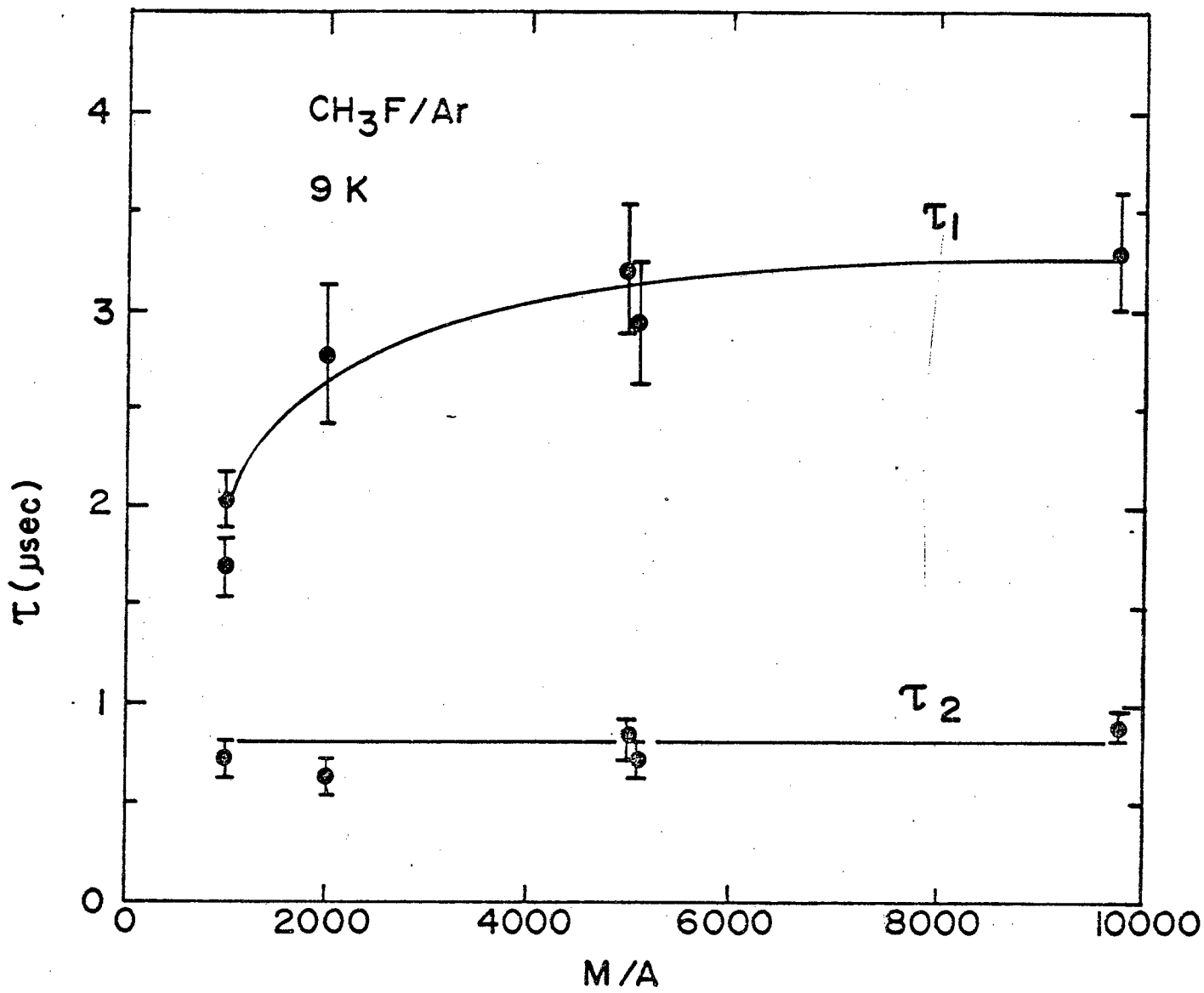


Fig. 9

This report was done with support from the Department of Energy. Any conclusions or opinions expressed in this report represent solely those of the author(s) and not necessarily those of The Regents of the University of California, the Lawrence Berkeley Laboratory or the Department of Energy.

Reference to a company or product name does not imply approval or recommendation of the product by the University of California or the U.S. Department of Energy to the exclusion of others that may be suitable.

TECHNICAL INFORMATION DEPARTMENT  
LAWRENCE BERKELEY LABORATORY  
UNIVERSITY OF CALIFORNIA  
BERKELEY, CALIFORNIA 94720